Relativistic ionization dynamics of hydrogenlike ions in strong electromagnetic fields: Generalized pseudospectral method for the time-dependent Dirac equation

Dmitry A. Telnov [1,*] and Shih-I Chu [2,3,†]

[1]*Department of Physics, St. Petersburg State University, 7-9 Universitetskaya nab., St. Petersburg 199034, Russia*
[2]*Center for Quantum Science and Engineering, and Center for Advanced Study in Theoretical Sciences,*
Department of Physics, National Taiwan University, Taipei 10617, Taiwan
[3]*Department of Chemistry, University of Kansas, Lawrence, Kansas 66045, USA*

We perform a theoretical and computational study of relativistic hydrogenlike ions subject to linearly polarized strong electromagnetic fields. The time-dependent Dirac equation is solved with the help of the generalized pseudospectral method in spherical coordinates. When solving the Dirac equation numerically with basis-set methods, spurious eigenstates usually show up. We suggest a simple transformation of the original discretized Dirac Hamiltonian that removes such states and keeps highly accurate true eigenstates. We calculate the ionization probabilities of the hydrogen atom and hydrogenlike ions Ne^{9+} and Ar^{17+} for various peak field strengths and pulse durations scaled with respect to the nuclear charge of the target. Calculations are performed both within and beyond the dipole approximation. We analyze the nondipole effects and find the region of the Lorentz deflection parameter where the dipole approximation is still applicable.

I. INTRODUCTION

Recent decades brought new breakthroughs in the laser technologies making it possible to generate extremely intense short pulses and attracting much attention to the light-matter interaction phenomena both in the theory and experiment (see review papers [1,2] and references therein). With optical lasers at the intensities 10^{17}–10^{18} W/cm^2, interaction of electromagnetic radiation with matter already enters a relativistic regime, where electrons can reach relativistic velocities within one optical cycle. Numerous new phenomena, such as relativistic self-focusing in plasmas, relativistic multiphoton and tunneling recollision dynamics, laser-assisted electron-positron pair production, etc., can be possibly observed [2]. On the other hand, the most powerful free-electron laser facilities, such as the X-ray Free-Electron Laser (XFEL) [3] at Hamburg and the Linac Coherent Light Source (LCLS) [4] at Stanford, are expected to produce electromagnetic fields with extremely high brilliance and wavelengths down to 0.05 nm, thus providing opportunities to explore the interaction of strong and short-wavelength electromagnetic radiation with highly charged ions, which themselves are relativistic quantum systems. In this respect, we can mention the upcoming High-Intensity Laser Ion-Trap Experiment (HILITE) experiment [5–7] intended to study the light-matter interaction using a Penning trap.

Theoretical treatment of highly charged ions exposed to electromagnetic fields with extremely high intensities must be fully relativistic since the electron moves with very high speed under the influence of both the Coulomb field of a highly charged nucleus and a strong external electromagnetic field. Various approaches for relativistic treatment of the laser-ion interaction have been suggested and implemented. We can mention several methods to solve the time-dependent Dirac equation (TDDE) numerically in spherical coordinates with expansion of the angular part of the wave function in spherical harmonics [8–13]. The radial wave function can be either discretized on the exponential mesh [8,14] or expanded on a basis of *B*-splines [9–13]. Kinetically balanced *B*-spline basis sets in both radial and angular coordinates for TDDE with an axial symmetry were introduced in Ref. [15]. Non-Hermitian approaches such as complex rotation of the coordinates, which have become a powerful tool in the theoretical atomic, molecular, and optical physics (see, for example, review papers [16,17]) are applied as well. The methods of Refs. [8,10] make use of the complex scaling of the coordinates, and complex absorbing potentials are utilized in Refs. [11,12]. Other theoretical and computational approaches feature the relativistic time-dependent close-coupling method [18,19], relativistic generalization of the matrix iteration method [20], and classical relativistic phase-space averaging method, generalized to arbitrary central potentials [21]. The relativistic Coulomb-corrected strong-field approximation [22,23] has been used for treatment of above-threshold ionization.

For the frequencies of the external electromagnetic fields in the ultraviolet region and below, where the wavelength of the radiation exceeds the atomic size to a great extent, the electric-dipole approximation is a common approach to describe the interaction of the atom or ion with the field. In the dipole approximation, the variation of the external field vector potential in space is neglected. Then the external field is a time-dependent and spatially uniform electric field, while the

―――――――
*d.telnov@spbu.ru
†sichu@ku.edu

magnetic field totally vanishes. This approximation has been widely used in nonrelativistic calculations of atoms in strong laser fields where the treatment is based on the time-dependent Schrödinger equation (TDSE). It was also applied on several occasions to essentially relativistic systems described by TDDE, such as highly charged ions exposed to electromagnetic fields [9,13,15,18,24]. However, nondipole effects due to magnetic fields may be important even at long wavelengths, depending on the field intensity [25]. When the intensity of the laser field increases, so does the velocity of the rescattering electron. Then the nondipole effects due to the magnetic field of the laser pulse become more and more important, and the dipole approximation eventually breaks down. Description of the interaction with the external electromagnetic field beyond the dipole approximation may be necessary even if an atomic or molecular system is treated nonrelativistically with TDSE [26–29]. For relativistic atomic and molecular systems, various approaches were made to extend the treatment beyond the dipole approximation in TDDE [8,10–12,19,30]. They include the Fourier [8], power series [11], and spherical Bessel function [19] expansions to accommodate the nondipole corrections. It was shown [10] that the spatial dependence in the pulse envelope, rather than in the carrier, provides a dominant correction beyond the dipole approximation.

In our previous work [30], we studied ionization of relativistic quasimolecular systems in strong fields solving the TDDE with the help of the generalized pseudospectral (GPS) method in prolate spheroidal coordinates. We found that spurious eigenstates of the Dirac Hamiltonian, which usually emerge among the true bound states when solving the problem with basis-set expansion methods, do not show up if the GPS method is applied in *prolate spheroidal coordinates*. In the present paper, we address the problem of strong-field ionization of relativistic hydrogenlike ions, where the spherical coordinates is the natural choice. Previously, the GPS method in spherical coordinates was successfully applied to a number of nonrelativistic atomic problems (see, for example, Ref. [17] and references therein). It does not require computations of the potential-energy matrix elements, and its nonuniform spatial grid is well suited for treatment of the systems bound by the Coulomb forces. It allows us to obtain highly accurate results while using only a moderate number of grid points. Therefore, it is desirable to extend this method to relativistic atomic systems described by the Dirac equation. However, if the GPS method in spherical coordinates is applied straightforwardly to the time-independent Dirac equation, then the spurious states do appear, and they may interfere in solving the TDDE as well. Here we suggest a modification of the discretized Dirac Hamiltonian that removes the spurious states while maintaining a high accuracy of true bound states. This method is applied to calculate the ionization probabilities of the hydrogen atom as well as hydrogenlike ions Ne^{9+} and Ar^{17+} subject to pulses of electromagnetic field with appropriately scaled parameters. The calculations are performed both within and beyond the dipole approximation. We analyze the relativistic ionization dynamics of hydrogenlike ions in strong electromagnetic fields and draw conclusions about the applicability of the dipole approximation.

The paper is organized as follows: In Sec. II, we present theoretical and computational details of our approach, which makes use of the GPS method in spherical coordinates. Here we extend this method for the accurate and efficient numerical solution of TDDE and suggest a modification of the Hamiltonian matrix to remove the spurious states. In Sec. III, we present and discuss our results regarding ionization dynamics of relativistic hydrogenlike ions in strong electromagnetic fields. In Sec. III B, we study the dependence of the ionization probabilities on the pulse duration and nuclear charge within the dipole approximation. In Sec. III C, the results obtained beyond the dipole approximation are presented and conclusions about the applicability of the dipole approximation are made. Section IV contains concluding remarks. Atomic units (a.u.) are used throughout the paper unless specified otherwise.

II. THEORETICAL AND COMPUTATIONAL METHODS

A. Time-dependent Dirac equation for one-electron system in linearly polarized electromagnetic field

A conventional form of the unperturbed Dirac Hamiltonian for an electron moving in the potential of the atomic nucleus is as follows:

$$H_D = c(\boldsymbol{\alpha} \cdot \boldsymbol{p}) + m_e c^2 \beta + U(r), \qquad (1)$$

where c is the speed of light, $\boldsymbol{p}$ is the momentum operator, m_e is the electron mass ($m_e = 1$ in atomic units), $U(r)$ is the nucleus potential, and $\boldsymbol{\alpha}$ and β are the Dirac matrices:

$$\boldsymbol{\alpha} = \left\| \begin{matrix} 0_2 & \boldsymbol{\sigma} \\ \boldsymbol{\sigma} & 0_2 \end{matrix} \right\|, \quad \beta = \left\| \begin{matrix} 1_2 & 0_2 \\ 0_2 & -1_2 \end{matrix} \right\|. \qquad (2)$$

In Eq. (2), "0_2" and "1_2" are 2×2 matrices:

$$0_2 = \begin{pmatrix} 0 & 0 \\ 0 & 0 \end{pmatrix}, \quad 1_2 = \begin{pmatrix} 1 & 0 \\ 0 & 1 \end{pmatrix}, \qquad (3)$$

and $\boldsymbol{\sigma}$ denotes the vector consisting of the Pauli matrices as components:

$$\sigma_x = \begin{pmatrix} 0 & 1 \\ 1 & 0 \end{pmatrix}, \quad \sigma_y = \begin{pmatrix} 0 & -i \\ i & 0 \end{pmatrix}, \quad \sigma_z = \begin{pmatrix} 1 & 0 \\ 0 & -1 \end{pmatrix}. \qquad (4)$$

From the very beginning, it is convenient to perform a unitary transformation:

$$H_0 = G^\dagger H_D G, \qquad (5)$$

$$G = \left\| \begin{matrix} C & 0_2 \\ 0_2 & iC \end{matrix} \right\|, \qquad (6)$$

where C is a diagonal 2×2 matrix:

$$C = \begin{pmatrix} 1 & 0 \\ 0 & \exp(i\varphi) \end{pmatrix} \qquad (7)$$

and φ is the azimuthal angle describing rotation about the z axis. For the unperturbed hydrogenlike ion, the choice of the z axis is arbitrary, since the core potential $U(r)$ is spherically symmetric. However, if a linearly polarized external electromagnetic field is introduced in the time-dependent problem, then the direction of the z axis is chosen along the polarization vector of the external field. The new Hamiltonian H_0 takes the

form

$$H_0 = m_e c^2 \left\| \begin{matrix} 1_2 & 0_2 \\ 0_2 & -1_2 \end{matrix} \right\| + c \left\| \begin{matrix} 0_2 & B \\ B^\dagger & 0_2 \end{matrix} \right\|$$

$$+ c \left\| \begin{matrix} 0_2 & D \\ D^\dagger & 0_2 \end{matrix} \right\| + U(r) \left\| \begin{matrix} 1_2 & 0_2 \\ 0_2 & 1_2 \end{matrix} \right\|. \tag{8}$$

Using the cylindrical coordinates ρ, φ, z as generic coordinates emphasizing the direction along the z axis, the 2×2 matrices B and D are expressed as follows:

$$B = \begin{pmatrix} \dfrac{\partial}{\partial z} & \dfrac{\partial}{\partial \rho} + \dfrac{1}{\rho} \\ \dfrac{\partial}{\partial \rho} & -\dfrac{\partial}{\partial z} \end{pmatrix}, \quad D = \begin{pmatrix} 0 & -\dfrac{i}{\rho}\dfrac{\partial}{\partial \varphi} \\ \dfrac{i}{\rho}\dfrac{\partial}{\partial \varphi} & 0 \end{pmatrix}. \tag{9}$$

They are anti-Hermitian:

$$B^\dagger = -B, \quad D^\dagger = -D. \tag{10}$$

Note that all terms in the unperturbed Hamiltonian H_0 are real-valued, except for the one with the matrix D.

The time-dependent Dirac equation for the electron interacting with the atomic core and external electromagnetic field reads as

$$i \frac{\partial}{\partial t} \Psi(\mathbf{r}, t) = (H_0 + V) \Psi(\mathbf{r}, t), \tag{11}$$

where $\Psi(\mathbf{r}, t)$ is a four-component wave function and the minimal coupling interaction of the electron with the external electromagnetic field linearly polarized along the z axis is described by the following term:

$$V(\mathbf{r}, t) = A(\mathbf{r}, t) \left\| \begin{matrix} 0_2 & i\sigma_z \\ -i\sigma_z & 0_2 \end{matrix} \right\| \tag{12}$$

[the vector is potential of the external field is equal to $A(\mathbf{r}, t)\hat{z}$, $\hat{z}$ being the unit vector along the z axis].

As a function of the azimuthal angle φ, the wave function Ψ can be expanded in the Fourier series:

$$\Psi = \sum_{m=-\infty}^{\infty} \exp(im\varphi) \Psi^{(m)}. \tag{13}$$

Each term on the right-hand side of Eq. (13) corresponds to the projection $M = m + 1/2$ of the total angular momentum on the z axis. The following relation holds:

$$H_0 \Psi = \sum_{m=-\infty}^{\infty} \exp(im\varphi) H_0^{(m)} \Psi^{(m)}. \tag{14}$$

The partial Hamiltonians $H_0^{(m)}$ are real-valued:

$$H_0^{(m)} = T_m + U(r) \left\| \begin{matrix} 1_2 & 0_2 \\ 0_2 & 1_2 \end{matrix} \right\|, \tag{15}$$

where T_m is the kinetic and rest energy operator:

$$T_m = m_e c^2 \left\| \begin{matrix} 1_2 & \dfrac{W_m}{m_e c} \\ \dfrac{W_m^\dagger}{m_e c} & -1_2 \end{matrix} \right\|, \tag{16}$$

$$W_m = B + D_m, \tag{17}$$

and the 2×2 matrices D_m are defined as follows:

$$D_m = \begin{pmatrix} 0 & \dfrac{m}{\rho} \\ -\dfrac{m}{\rho} & 0 \end{pmatrix}. \tag{18}$$

Since the unperturbed Hamiltonian H_0 is spherically symmetric, the projection of the total angular momentum on the z axis is conserved if the external field is switched off. This is also the case when the interaction with the laser field is treated in the dipole approximation and the field is linearly polarized along the z axis. Then for the initial state with the definite angular-momentum projection, only one term with the corresponding m value should be retained in Eqs. (13) and (14). Beyond the dipole approximation, several m terms in the wave-function expansion (13) must be kept to achieve convergence. In general, the stronger the field, the larger number of angular-momentum projections should be used.

To accomplish the time propagation in Eq. (11), we apply the split-operator method in the energy representation [31], which we have extensively used for solving the TDSE [32–34] and time-dependent Kohn-Sham equations [35–37] as well as to solve the TDDE for quasimolecules in prolate spheroidal coordinates [30]. The following short-time propagator scheme is employed:

$$\Psi(t + \Delta t) = \exp\left(-\frac{i}{2}\Delta t \, H_0\right)$$

$$\times \exp\left[-i\Delta t \, V\left(t + \frac{1}{2}\Delta t\right)\right]$$

$$\times \exp\left(-\frac{i}{2}\Delta t \, H_0\right) \Psi(t); \tag{19}$$

at each time step, an error bound of this scheme is of the order of $(\Delta t)^3$. The field-free propagator $\exp(-\frac{i}{2}\Delta t \, H_0)$ is time independent; it is calculated only once before the time propagation process begins. The total field-free propagator can be expressed through the propagators corresponding to the specific angular-momentum projections:

$$\exp\left(-\frac{i}{2}\Delta t \, H_0\right) \Psi(t)$$

$$= \sum_{m=-\infty}^{\infty} \exp(im\varphi) \exp\left(-\frac{i}{2}\Delta t \, H_0^{(m)}\right) \Psi^{(m)}(t). \tag{20}$$

The partial propagators $\exp(-\frac{i}{2}\Delta t \, H_0^{(m)})$ are calculated by the spectral expansion:

$$\exp\left(-\frac{i}{2}\Delta t \, H_0^{(m)}\right) = \sum_n \exp\left(-\frac{i}{2}\Delta t \, E_n^{(m)}\right) \left| \Psi_n^{(m)} \right\rangle \left\langle \Psi_n^{(m)} \right|, \tag{21}$$

where $\Psi_n^{(m)}$ and $E_n^{(m)}$ are the eigenstates and energies of the partial Hamiltonian $H_0^{(m)}$ (15). Equation (20) is very useful for the calculations beyond the dipole approximation where the angular-momentum projection is not conserved: in the matrix-vector product, it allows us to use several matrices of a smaller dimension (partial propagators) rather than one matrix of a larger dimension (full propagator).

The external field propagator $\exp(-i\Delta t \, V)$ can be calculated analytically for the interaction operator given by

Eq. (12):

$$\exp(-i\Delta t\, V) = \left\| \begin{matrix} \cos(A\Delta t)1_2 & \sin(A\Delta t)\sigma_z \\ -\sin(A\Delta t)\sigma_z & \cos(A\Delta t)1_2 \end{matrix} \right\|. \quad (22)$$

In the full coordinate representation, where the angle φ is discretized on a uniform grid, it is quasidiagonal in the sense that it consists of four square blocks, each of them being a diagonal matrix (note that multiplication by a function of the coordinates is represented by a diagonal matrix in the GPS method that we apply to solve the problem). The field propagator is time dependent and must be calculated at each time step. However, this operation is not time consuming since the propagator matrix is quasidiagonal. Before applying the partial field-free propagators at each time step, the wave function must be converted from the full coordinate representation to the angular-momentum projection representation; this is done by the fast Fourier transform (FFT) with respect to the coordinate φ. This operation is performed by the hardware-optimized FFT routines and is not time consuming, either.

The split-operator formula (19) is not exact but approximate because the operators H_0 and V do not commute. Since the field propagator (22) couples the positive and negative energy states with the large energy gap $2m_e c^2$ between them, the commutator $[H_0, V]$ effectively multiples the states by this factor, and the time step Δt in the split-operator method must be chosen small enough to suppress the influence of the commutator. The requirement that the time step must be very small could be a serious disadvantage when applying the split-operator method to solve the TDDE. We should note here that the stiffness issues are known for the TDDE and have been discussed in the literature [11,20,38]. In our calculations, converged results in the TDDE propagation using the split-operator method can be obtained with the time step about two orders of magnitude smaller than the time step in the TDSE propagation for the same system and field parameters. An alternative time propagation scheme is based on the Crank-Nicolson algorithm [39]. In this method, the Hamiltonian is not split in two parts, the commutator problem does not exist, and the time step can be chosen much larger than that in the split-operator method. However, one has to deal with the large Hamiltonian matrix obtained by discretization of all three coordinates (including the angle φ) because the total Hamiltonian beyond the dipole approximation does not possess the axial symmetry.

B. Generalized pseudospectral discretization of the Dirac Hamiltonian in spherical coordinates and removal of spurious states

To obtain the initial wave function in the time-dependent problem (11) and construct the field-free propagators (21), one has to solve the eigenvalue problems for the partial unperturbed Hamiltonians (15):

$$H_0^{(m)}\Psi_n^{(m)} = E_n^{(m)}\Psi_n^{(m)}. \quad (23)$$

We use the GPS method in the spherical polar coordinates suitable for one-center atomic targets [36]. The radial coordinate r is discretized by using the Gauss-Lobatto scheme where the collocation points are the roots of the polynomial $(1-x^2)P'_{N_x+1}(x)$, $P'_{N_x+1}(x)$ being the derivative of the

Legendre polynomial. There are $N_x + 2$ collocation points within the interval $[-1, 1]$, including the points -1 and 1. The latter two points correspond to the boundaries of the radial coordinate range when an appropriate mapping between x and r is established. If zero boundary conditions are imposed on the wave function at these points, only N_x internal collocations points are used to represent the discretized wave function. We adopt the following mapping function $r(x)$:

$$r(x) = R_m \frac{(1+x)^2 + 2\delta(1+x)}{1 - x + 4R_m(1+\delta)/R_b}. \quad (24)$$

Here R_m, R_b, and δ are parameters of the transformation. The endpoint R_b must be chosen large enough to ensure the space domain used to solve the equation contains all important physics. A quadratic term in the numerator of Eq. (24) and a small value of the parameter δ make the distribution of the radial grid points denser in the vicinity of the nucleus; this is important for the calculations of heavy ions where the extended nucleus model is used.

For the polar angle ϑ, we apply the Gauss-Legendre discretization scheme where the collocation points are the roots of the Legendre polynomial $P_{N_y}(y)$. There are N_y collocation points which lie entirely within the interval $[-1, 1]$. An appropriate mapping transformation $\vartheta(y)$ is given by the following expression:

$$\vartheta = \frac{\pi}{2}(1 + y). \quad (25)$$

It is convenient to introduce an array $\Phi_{ij}^{(m)}$ containing the scaled values of the wave function $\Psi^{(m)}(r, \vartheta)$ at the collocation points:

$$\Psi^{(m)}(r_i, \vartheta_j)$$
$$= \frac{1}{r_i}\sqrt{\frac{(N_x+1)(N_x+2)\left(1-y_j^2\right)}{8\pi r_i'\vartheta_j'\sin\vartheta_j}} P_{N_x+1}(x_i)P'_{N_y}(y_j)\Phi_{ij}^{(m)} \quad (26)$$

(r_i' and ϑ_j' denote the values of the derivatives dr/dx and $d\vartheta/dy$ at the collocation points x_i and y_j, respectively). Then the normalization integral of the wave function is calculated as follows:

$$\int d^3r [\Psi^{(m)}(\boldsymbol{r})]^\dagger \Psi^{(m)}(\boldsymbol{r}) = \sum_{i=1}^{N_x}\sum_{j=1}^{N_y}\left[\Phi_{ij}^{(m)}\right]^\dagger \Phi_{ij}^{(m)}. \quad (27)$$

Upon discretization, the differential operators with respect to the coordinates in the Hamiltonian [see Eq. (9)] are represented by matrices acting upon the vector with the components $\Phi_{ij}^{(m)}$. The matrix elements are calculated as follows:

$$\left(\frac{\partial}{\partial z}\right)_{ij, i'j'} = \frac{\delta_{jj'}}{\sqrt{r_i' r_{i'}'}}\cos\vartheta_j d_{ii'}^x$$

$$- \frac{\delta_{ii'}}{2r_i\sqrt{\vartheta_j'\vartheta_{j'}'}}\left(\sqrt{\frac{1-y_{j'}^2}{1-y_j^2}}\sqrt{\frac{\sin\vartheta_j}{\sin\vartheta_{j'}}}\sin\vartheta_j d_{jj'}^y\right.$$

$$\left. - \sqrt{\frac{1-y_j^2}{1-y_{j'}^2}}\sqrt{\frac{\sin\vartheta_{j'}}{\sin\vartheta_j}}\sin\vartheta_{j'} d_{j'j}^y\right), \quad (28)$$

$$
\left(\frac{\partial}{\partial\rho}\right)_{ij,i'j'} = \frac{\delta_{jj'}}{\sqrt{r_i'r_{i'}'}}\sin\vartheta_j d_{ii'}^x
$$
$$
+ \frac{\delta_{ii'}}{2r_i\sqrt{\vartheta_j'\vartheta_{j'}'}}\left(\sqrt{\frac{1-y_{j'}^2}{1-y_j^2}}\sqrt{\frac{\sin\vartheta_j}{\sin\vartheta_{j'}}}\cos\vartheta_j d_{jj'}^y\right.
$$
$$
\left.- \sqrt{\frac{1-y_j^2}{1-y_{j'}^2}}\sqrt{\frac{\sin\vartheta_{j'}}{\sin\vartheta_j}}\cos\vartheta_{j'} d_{j'j}^y\right) - \frac{\delta_{ii'}\delta_{jj'}}{2r_i\sin\vartheta_j},
$$
$$
(29)
$$

with the derivative matrices $d_{ii'}^x$ and $d_{jj'}^y$ defined as

$$
d_{ii'}^x = \frac{1}{x_i - x_{i'}} \; (i \neq i'), \quad d_{ii}^x = 0 \; (1 \leqslant i \leqslant N_x); \quad (30)
$$

$$
d_{jj'}^y = \frac{1}{y_j - y_{j'}} \; (j \neq j'), \quad d_{jj}^y = \frac{y_j}{1 - y_j^2}. \quad (31)
$$

The nuclear potential and other multiplications by functions of the coordinates in the Hamiltonian are represented by diagonal matrices in the GPS method, with the matrix elements equal to the values of the potential at the collocation points.

It is well known that the numerical solution of the eigenvalue problem for the Dirac equation using basis-set expansions leads to emergence of spurious eigenstates among the true bound states in the discrete spectrum region [40]. Various methods have been suggested to remove such undesirable states; from imposing special boundary conditions [41,42] to using kinetically balanced basis sets [43]. When working with B-spline basis sets, it was shown that spurious states are eliminated if splines of different orders are used for the large and small components of the wave function [44]. Other based on B splines numerical schemes, which are free of the spurious states, were suggested in Ref. [45]. It was also reported that nonphysical states are removed when using the split-shift potential method for the radial Dirac equation [46]. In the previous study [30] we reported that spurious states do not show up, at least among the low-lying bound states, when the GPS method is applied in prolate spheroidal coordinates. When the GPS method is applied in spherical coordinates for an eigenvalue problem with a spherically symmetric potential, the spurious states do appear. To get rid of the spurious states, we suggest here a transformation of the Hamiltonian matrix in the spirit of the dual kinetic balance (DKB) approach [43]. First, the following substitution is applied for the wave function:

$$
\Psi^{(m)} = Q_m \widetilde{\Psi}^{(m)}, \quad (32)
$$

with the matrix Q_m defined as follows:

$$
Q_m = \left\|\begin{array}{cc} 1_2 & -\dfrac{W_m}{2m_ec} \\ \dfrac{W_m^\dagger}{2m_ec} & 1_2 \end{array}\right\|. \quad (33)
$$

To make the eigenvalue problem symmetric for the wave function $\widetilde{\Psi}_n^{(m)}$, Eq. (23) should be also multiplied by $Q_m^\dagger$:

$$
Q_m^\dagger H_0^{(m)} Q_m \widetilde{\Psi}_n^{(m)} = E_n^{(m)} Q_m^\dagger Q_m \widetilde{\Psi}_n^{(m)}. \quad (34)
$$

Of course, if the discretized versions of $H_0^{(m)}$ and Q_m are used in Eq. (34), this congruence matrix transformation of Eq. (23) does not change the eigenvalues, and the eigenvectors are related to each other by a nonsingular matrix in Eq. (32), so the spurious states are not removed. The key point is to calculate the operator product analytically *before* the discretization is applied. For the kinetic and rest energy part of the Hamiltonian T_m the result is as follows:

$$
Q_m^\dagger T_m Q_m = m_ec^2\left\|\begin{array}{cc} 1_2 + \dfrac{3W_mW_m^\dagger}{(2m_ec)^2} & -\dfrac{2W_mW_m^\dagger W_m}{(2m_ec)^3} \\ -\dfrac{2W_m^\dagger W_m W_m^\dagger}{(2m_ec)^3} & -1_2 - \dfrac{3W_m^\dagger W_m}{(2m_ec)^2} \end{array}\right\|. \quad (35)
$$

The operator product $W_mW_m^\dagger = W_m^\dagger W_m$ is a block-diagonal matrix:

$$
W_mW_m^\dagger = \begin{pmatrix} -\Delta_{\rho z} + \dfrac{m^2}{\rho^2} & 0 \\ 0 & -\Delta_{\rho z} + \dfrac{(m+1)^2}{\rho^2} \end{pmatrix}, \quad (36)
$$

where $\Delta_{\rho z}$ is a part of the Laplace operator:

$$
\Delta_{\rho z} = \frac{\partial^2}{\partial\rho^2} + \frac{1}{\rho}\frac{\partial}{\partial\rho} + \frac{\partial^2}{\partial z^2}. \quad (37)
$$

Upon discretization, this operator is *not expressed* through a simple matrix product of the derivative matrices (28) and (29). The zero boundary conditions at $r = 0$ and $r = R_b$ presumed by the matrices (28) and (29) may not be satisfied upon the first differentiation; for the same reason, the centrifugal terms in Eq. (36) cannot be correctly reproduced by numerical differentiation with the matrices (28) and (29). The correct discretized form of $\Delta_{\rho z}$ reads as

$$
(\Delta_{\rho z})_{ij,i'j'} = -\frac{\delta_{jj'}}{\sqrt{r_i'r_{i'}'}}\sum_{k=0}^{N_x+1}\frac{d_{ki}^x d_{ki'}^x}{r_k'}
$$
$$
- \frac{\delta_{ii'}}{r_i^2\sqrt{\vartheta_j'\vartheta_{j'}'}}\sqrt{\frac{(1-y_j^2)(1-y_{j'}^2)}{\sin\vartheta_j \sin\vartheta_{j'}}}
$$
$$
\times \sum_{k=1}^{N_y}\frac{\sin\vartheta_k d_{kj}^y d_{kj'}^y}{\vartheta_k'(1-y_k^2)}. \quad (38)
$$

Note that the summation for the radial part of this matrix includes the endpoints $k = 0$ and $k = N_x + 1$, which are omitted in the first derivative matrices (28) and (29) because of the zero boundary conditions imposed on the wave function.

With the Laplace operator in the product $W_mW_m^\dagger$, one may hope that spurious states disappear from the solution of the discretized eigenvalue problem; this is the case for the time-independent Schrödinger equation where the kinetic energy is expressed through the Laplace operator: the discretized eigenvalue problem returns no spurious states. Calculation of the operator product $W_mW_m^\dagger$ according to Eq. (36) is indeed crucial for removal of spurious states, but only in the diagonal blocks of the matrix (35). The off-diagonal blocks with the product of three W_m matrices can be calculated by matrix multiplication with the discretized first-derivative matrices. Upon this transformation of the Hamiltonian, spurious eigenstates do not

emerge when solving the eigenvalue problem (34). However, Eq. (34) is not a standard but generalized eigenvalue problem. The nuclear potential term is also transformed, making it not very convenient to solve both the time-independent and time-dependent problems. To avoid such complications, we now apply the inverse transformation with the *discretized* matrix Q_m:

$$\widetilde{T}_m = \left[\bar{Q}_m^{-1}\right]^\dagger [Q_m^\dagger T_m Q_m] \bar{Q}_m^{-1}. \tag{39}$$

We emphasize that the discretized kinetic and rest energy matrix $\widetilde{T}_m$ on the left-hand side of Eq. (39) is not equal to the discretized version of the original matrix (16) because the transformation on the right-hand side of Eq. (39) is not an identical one. The product $Q_m^\dagger T_m Q_m$ is *first calculated analytically* according to Eq. (35) and *then discretized* while the matrix $\bar{Q}_m^{-1}$ is obtained numerically by the matrix inversion procedure from the discretized Q_m. After all these manipulations, the Hamiltonian $H_0^{(m)}$ is modified from its original form. The new discretized Hamiltonian is a sum of $\widetilde{T}_m$ and the potential term:

$$\widetilde{H}_0^{(m)} = \widetilde{T}_m + U(r) \left\| \begin{matrix} 1_2 & 0_2 \\ 0_2 & 1_2 \end{matrix} \right\|, \tag{40}$$

and we go back to the standard eigenvalue problem for the wave functions $\Psi_n^{(m)}$:

$$\widetilde{H}_0^{(m)} \Psi_n^{(m)} = E_n^{(m)} \Psi_n^{(m)}. \tag{41}$$

Compared to the directly discretized original eigenvalue problem (23), Eq. (41) returns the physical eigenstates but no spurious states.

C. Extended nucleus potential and vector potential of the laser field

For the hydrogen atom, we neglect the finite size of the nucleus and use the Coulomb interaction potential:

$$U(r) = -\frac{Z}{r}, \tag{42}$$

with the charge Z equal to 1. For heavier hydrogenlike ions, however, more realistic extended nucleus models should be used where the interaction potential is determined by the distribution of the nuclear charge $\rho_n(r)$:

$$U(r) = -\int d^3 r' \frac{\rho_n(r')}{|\boldsymbol{r} - \boldsymbol{r}'|}. \tag{43}$$

In this study, we make use of the spherical-symmetric Fermi nuclear charge distribution [47,48]:

$$\rho_n(r) = \rho_0 \frac{1 + \exp[-r_0/b]}{1 + \exp[(r - r_0)/b]}, \tag{44}$$

where the parameter b is set to $2.3/(4 \ln 3)$ fm (see Ref. [47]) and parameters ρ_0 and r_0 are calculated given the total nucleus charge Z and experimental values of the nucleus root-mean-square radius [49]. Note that the potential (43) with the smooth nuclear charge distribution (44) does not have a Coulomb singularity at $r = 0$, hence the Dirac wave function is also regular there. This is important for numerical calculations with highly charged nuclei; in this case, when the Coulomb potential (42) is used, the accuracy may not be good

enough if one does not specifically account for the singularity of the wave function.

Interaction with the external electromagnetic field is described by Eq. (12). The field is linearly polarized along the z axis and propagates along the x axis; we adopt the Gaussian shape of the laser pulse:

$$A(\boldsymbol{r}, t) = \frac{cF}{\omega} \exp\left[-2 \ln 2 \left(\frac{t - x/c}{\tau}\right)^2\right] \sin\left(\omega t - \frac{\omega x}{c}\right), \tag{45}$$

where F is the peak electric-field strength, ω is the carrier frequency, and τ has a meaning of the full width at half maximum (FWHM) in the *intensity* (or A^2) profile. Equation (45) describes the general case beyond the dipole approximation. In the dipole approximation, the dependence of the vector potential on the coordinate x is dropped:

$$A(t) = \frac{cF}{\omega} \exp\left[-2 \ln 2 \left(\frac{t}{\tau}\right)^2\right] \sin \omega t. \tag{46}$$

III. RESULTS AND DISCUSSION

A. Hydrogenlike ions and nonrelativistic scaling with respect to the nuclear charge

We have performed calculations of the ionization probabilities for the hydrogen atom and two hydrogenlike ions Ne^{9+} and Ar^{17+} subject to strong pulses of electromagnetic radiation. It is well known that the TDSE for one-electron atomic ions where the interaction of the electron with the nucleus is described by the exact Coulomb potential satisfies exact scaling relations with respect to the nuclear charge Z. This is true not only for unperturbed Coulomb systems but also for hydrogenlike ions interacting with external electromagnetic fields in the dipole approximation [50]. A proper scaling of the spatial and time variables as well as pulse parameters in the equation will convert the equation for the ion with the nuclear charge Z into the equation for the hydrogen atom ($Z = 1$). This nonrelativistic scaling is achieved by the following substitutions:

$$\boldsymbol{r} = \tilde{\boldsymbol{r}}/Z, \quad t = \tilde{t}/Z^2, \quad \omega = \tilde{\omega} Z^2, \quad F = \tilde{F} Z^3, \tag{47}$$

where the variables and parameters with tilde correspond to the H atom. Without the external field ($F = 0$), the electronic energy eigenvalues of the unperturbed ions with different Z scale as Z^2. *Exact* scaling with the nuclear charge does not hold for relativistic systems described by the TDDE, although some approximate relations have been suggested [9,13]. Strictly speaking, the scaling (47) does not hold exactly even for the TDSE, if the electron-nucleus interaction is described within the extended nucleus model, and not by the exact Coulomb potential. However, because of the large difference between the electronic and nuclear length scales, the effect of the finite nucleus dimension on the electronic motion is very small, therefore the deviation from the nonrelativistic scaling relations caused by the finite nucleus size is insignificant. Then any differences between the TDDE results for the scaled systems (within the dipole approximation) may be attributed to relativistic effects, which are expected to grow with the increase of the nuclear charge Z. As discussed in Ref. [9] for multiphoton ionization of hydrogenlike ions, the main

TABLE I. Energies of the ground and low-lying excited states of
Ar^{17+} (in a.u.) for the total angular-momentum projection $M = 1/2$.
Column A gives the original Dirac Hamiltonian (15), spurious states
show up; column B gives the modified Dirac Hamiltonian (40), no
spurious states; column C give the relativistic exact Coulomb (point-
like nucleus) eigenvalues; column D gives the nonrelativistic exact
Coulomb (point-like nucleus) eigenvalues. The grid size is 128×16,
the computation box size $R_b = 3.33$ a.u.

State	A	B	C	D
$1s_{1/2}$	−162.70453	−162.70453	−162.70486	−162.0
Spurious	−41.027318			
$2p_{1/2}$	−40.720364	−40.720364	−40.720364	−40.50
$2s_{1/2}$	−40.720322	−40.720322	−40.720364	−40.50
$2p_{3/2}$	−40.543767	−40.543767	−40.543767	−40.50
Spurious	−22.721053			
$3p_{1/2}$	−18.078284	−18.078284	−18.078284	−18.00
$3s_{1/2}$	−18.078271	−18.078271	−18.078284	−18.00
$3p_{3/2}$	−18.025940	−18.025940	−18.025940	−18.00
$3d_{3/2}$	−18.025940	−18.025940	−18.025940	−18.00
$3d_{5/2}$	−18.008635	−18.008635	−18.008635	−18.00
Spurious	−13.726728			

effect is the downshift of the ground-state energy level in
the relativistic case resulting in somewhat smaller ionization
probabilities obtained for the scaled systems with larger Z.

For the GPS discretization of the radial coordinate, we
apply Eq. (24) with the following values of the parameters:

$$R_m = 30/Z \text{ a.u.}, \quad R_b = 60/Z \text{ a.u.}, \quad \delta = 0.02. \quad (48)$$

For each hydrogenlike target, the length parameters R_m and
R_b are scaled according to Eq. (47), and the dimensionless
parameter δ is not scaled.

In Table I, we present the binding energies of the ground
and low-lying excited states with the total angular-momentum
projection $M = 1/2$ of Ar^{17+} to illustrate how spurious states
are removed when using the modified Dirac Hamiltonian (40).
The calculations are performed with 128 radial and 16 angular
(ϑ) grid points. We note that the spurious eigenvalues in
column A correspond to the specific numerical parameters
listed in Eq. (48) and coordinate grid used. Unlike the true
eigenvalues, they are very sensitive to variations of the pa-
rameters. The effect of the extended nucleus model (splitting
between the $s_{1/2}$ and $p_{1/2}$ energy levels along with the upshift
of the s states) is seen when comparing columns B and C
(the latter contains exact relativistic energies for the point-like
nucleus). The magnitude of the relativistic corrections can be
estimated by comparison with the values in column D, which
are exact nonrelativistic energies of the electron bound in the
exact Coulomb potential. In all the calculations we use the
speed of light $c = 137.035999084$ a.u. (2018 CODATA [51]
recommended inverse fine-structure constant).

B. Strong-filed ionization of hydrogenlike ions in dipole approximation

In the dipole approximation, we have performed two
sets of calculations and examined the dependence of the

ionization probability on the pulse duration and nucleus
charge. First, we calculate the ionization probabilities of the
hydrogen atom for several pulse durations and peak field
strengths. The carrier frequency of the laser pulse in Eq. (46)
is fixed at 3.5 a.u., the same frequency was used in the recent
studies of the relativistic ionization dynamics of the hydrogen
atom [10,11]. The field strength range is 0 to 90 a.u. In all
our calculations we use 128 radial grid points and 16 angular
(ϑ) grid points. The radial coordinate endpoint $R_b = 60$ a.u.
is large enough to accommodate all ionization dynamics of
the hydrogen atom even at the strongest fields used in the
calculations. The classical excursion distance of the electron
in the laser field can be estimated as F/ω^2; at $F = 90$ a.u.,
this quantity is equal to 7.35 a.u., that is well below R_b. To
prevent spurious reflections of the electron wave packet from
the box boundary, we use an absorbing layer in the vicinity of
R_b. We checked the convergence with respect to the spatial (r
and ϑ) grid performing numerical tests changing the number
of grid points and the endpoint of the radial grid R_b. Increasing
the number of r grid points to 160 and ϑ grid points to 24 as
well as extending the radial box size to $R_b = 70$ a.u. changed
the ionization probabilities only slightly (the largest deviation
was in the third significant digit) even for strongest fields
used in the present calculations. We may conclude that with
the 128×16 coordinate grid and $R_b = 60$ a.u. both the bound
and pseudocontinuum states important for the processes under
consideration are represented well enough. Convergence of
the data with respect to the number of angular-momentum
projections in the calculations beyond the dipole approxima-
tion is discussed below in Sec. III C.

The calculations are performed for three values of the pulse
duration parameter τ in Eq. (46): 2.5, 3.75, and 5 optical
cycles (o.c.). Since we use the Gaussian pulse shape, the pulse
envelope function never turns zero, so the actual propagation
time should be chosen so that the field strength is negligi-
bly small at the beginning and end of the pulse. The actual
propagation times for the three values of the τ parameter
listed above are 10, 15, and 20 o.c., respectively. Finally, we
use 65 536 time steps per optical cycle in the split-operator
propagation method to make sure the results are converged
with respect to this parameter. If the Crank-Nicolson scheme
is used, good results can be obtained with much smaller num-
ber of times steps per optical cycle, 1024 or 2048. In all the
calculations the hydrogen atom is initially in the ground $1s_{1/2}$
state, and the ionization probability P_i is calculated as

$$P_i = 1 - P_b, \quad (49)$$

where P_b is the total population of bound states at the end of
the time propagation.

Figure 1 displays the ionization probabilities of the hydro-
gen atom versus the peak field strength for different pulse
durations. When the external field is weak, the ionization
probability rapidly increases with the field strength. However,
this pattern ends around $F = 10$ a.u. All three curves exhibit
a local maximum; the position of the maximum changes only
slightly with the pulse duration: $F = 14$ a.u. for $\tau = 2.5$ o.c.,
$F = 13$ a.u. for $\tau = 3.75$ o.c., and $F = 12$ a.u. for $\tau = 5$ o.c.
As the field strength further increases, the local maximum is
followed by a local minimum. The minimum is very shallow
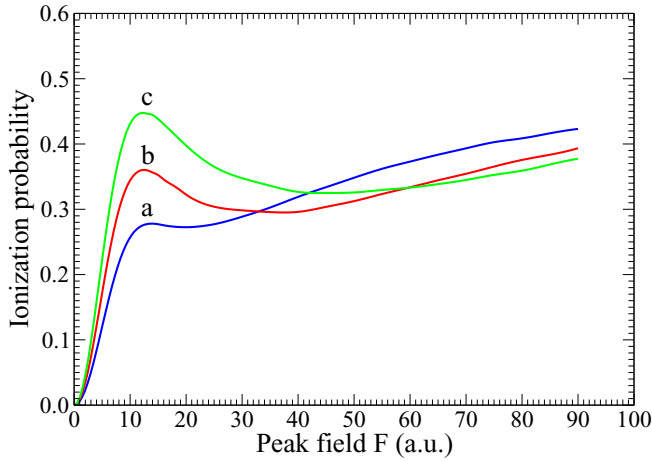for the shortest pulse ($\tau = 2.5$ o.c.) and becomes deeper as the

FIG. 1. Ionization probabilities of the hydrogen atom versus the peak field strength in the dipole approximation. The laser pulse is Gaussian with the carrier frequency $\omega = 3.5$ a.u. and different durations: (a) $\tau = 2.5$ o.c., (b) $\tau = 3.75$ o.c., and (c) $\tau = 5$ o.c.
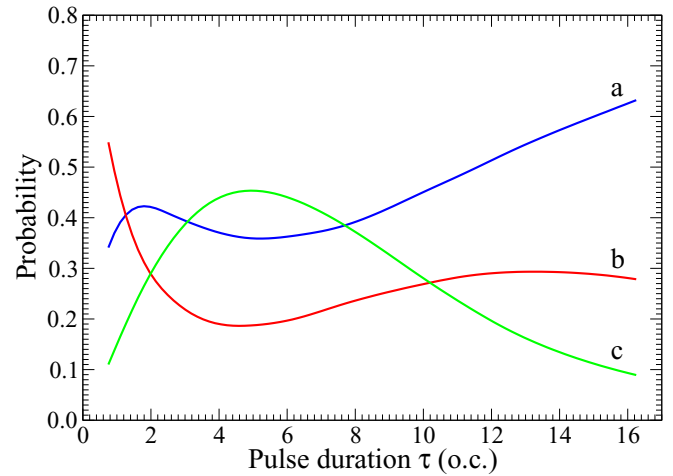

FIG. 2. (a) Ionization probability of the hydrogen atom, (b) population of the ground state after the pulse, and (c) population of the excited bound states after the pulse versus the pulse duration in the dipole approximation. The pulse shape is Gaussian and the peak field strength is $F = 80$ a.u.

pulse duration increases. The shape of the curve at $\tau = 5$ o.c. resembles that in Fig. 1 of Ref. [11] where the laser pulse with the sin^2 shape and duration of 15 o.c. was used. A counterintuitive behavior of the ionization probability, which decreases as the field strength increases is known as stabilization in superintense external fields [52]. We also point out another counterintuitive result shown in Fig. 1. Normally one expects that for the same carrier frequency and peak field strength the ionization probability increases with the pulse duration. As one can see in Fig. 1, this is the case for relatively weak fields only. Around $F = 35$ a.u., the pattern in the dependence of the ionization probability on the pulse duration begins to change; at the field strengths larger than 60 a.u., it is totally reversed: the shortest pulse features the largest ionization probability, and the longest pulse duration results in the smallest ionization probability. Regarding this observation, we have the following comments: First, such a behavior of the ionization probability with respect to the pulse duration is not specific for the relativistic dynamics only. Previously it was also observed in nonrelativistic calculations of the hydrogen atom subject to superintense laser pulses in the so-called dynamic stabilization regime [53,54]. Second, its observability depends strongly on the carrier frequency [53] and pulse shape [54]. A stronger effect is observed for the pulses with sharper edges, while for flatter pulse shapes a normal behavior of the ionization probability (increasing with the pulse duration) is detected. Finally, for the fixed peak field strength and carrier frequency, the counterintuitive dependence of the ionization probability on the pulse duration is restricted to some finite range of pulse durations. For long enough pulses, a normal dependence of the ionization probability on the pulse duration is restored [53,54]. As our calculations show, when the ionization probability decreases with increasing pulse duration, this happens mostly due to the population trapped in the excited bound states. Thus we may guess that a kind of interference mechanism is responsible for this phenomenon if the laser pulse is relatively short. Contributions to the transition amplitudes from the leading and trailing edges of the

pulse may interfere constructively for some interval of the excited bound-state energies. Then a substantial amount of the electronic population is trapped in such states and not transferred to the continuum after the laser pulse is switched off. In Fig. 2, we show the ionization probability of the hydrogen atom along with the populations of the ground and excited bound states after the pulse. The calculations are performed on a rather wide interval of the pulse duration parameter τ, 0.75 to 16.25 o.c., for a representative peak field strength of 80 a.u. where the anomalous dependence of the ionization probability on the pulse duration is detected. As one can see, the local minimum of the ionization probability at $\tau \approx 5$ o.c. corresponds to the local maximum of the excited bound-state population. Approximately at the same pulse duration, the ground-state population reaches a local minimum.

In Fig. 3 we show ionization probabilities of the hydrogen atom and two hydrogenlike ions Ne^{9+} and Ar^{17+}. For the H atom we use the same carrier frequency $\omega = 3.5$ a.u. and peak field strength range as discussed above. For the other targets, these parameters are scaled according to Eq. (47). The pulse duration τ is equal to 2.5 o.c. for all three targets. As one can see, in the weak-field region, approximately up to $F = 15Z^3$ a.u., the nonrelativistic scaling relations (47) work very well. The ionization probabilities of all three targets are very close to each other. Relativistic effects within the dipole approximation are small, and this is not surprising given that the nuclear charge of the ions is not very high. Still, the ionization probability of the ions (especially Ar^{17+}) is smaller than that of the hydrogen atom. This result can be understood since the ionization potentials of the relativistic hydrogenlike ions are larger than the scaled ionization potential of the nonrelativistic hydrogen atom. The nonrelativistic scaling apparently breaks down for the field strengths larger than $F = 20Z^3$ a.u., indicating a transition to the relativistic dynamics for the hydrogenlike ions in the scaled laser fields. For the hydrogen atom itself, the relativistic effects remain small even if the peak field strength is as large as 100 a.u. [11].
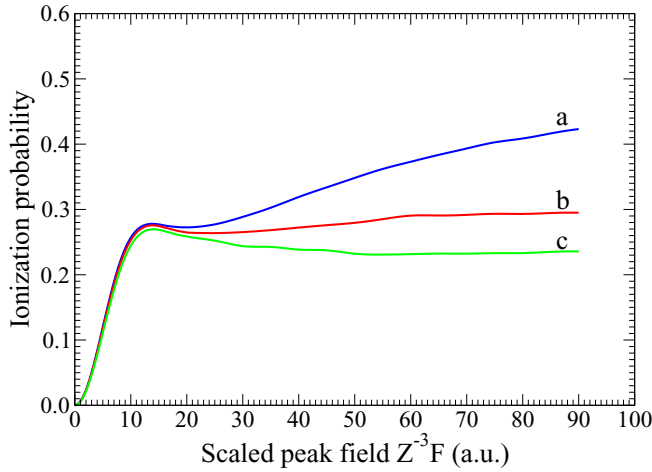
FIG. 3. Ionization probabilities of (a) H, (b) Ne^{9+}, and (c) Ar^{17+} versus the peak field strength in the dipole approximation. The laser pulse is Gaussian with the carrier frequency $\omega = 3.5Z^2$ a.u. and duration $\tau = 2.5$ o.c. for each target.

These effects are much more important for the hydrogenlike ions with sufficiently large nuclear charges. The peak value of the classical electron momentum in the laser field can be estimated as F/ω. At $F \approx 48$ a.u. it reaches the value 13.7, so the classical electron velocity v after ionization of the hydrogen atom is 10 times smaller than the speed of light. Since the relativistic dynamic effects are of the order of $(v/c)^2$, they are not very significant at this field strength. However, if the scaling (47) is applied, the classical electron momentum scales as Z. Then for Ne^{9+} it is 10 times larger, and for Ar^{17+} 18 times larger than that for the hydrogen, taking the ionization dynamics to the essentially relativistic regime. In this regime, the stabilization pattern in the dependence of the ionization probability on the scaled field strength seen in Fig. 3 for Ne^{9+} and Ar^{17+} at $F > 20Z^3$ a.u. is apparently different from that seen for the hydrogen atom. The ions with larger Z (that is, with larger electron velocities for the same scaled field strength) are more stable against ionization. We should note, however, that this range of the laser field strength actually lies beyond the applicability region of the dipole approximation for Ne^{9+} and Ar^{17+} (see Sec. III C).

C. Strong-field ionization of hydrogenlike ions beyond the dipole approximation

Increasing the external field strength will eventually lead to a failure of the dipole approximation. Depending on the carrier frequency, this approximation may become very inaccurate even if the external field is not extremely strong. A breakdown of the dipole approximation is caused mainly by the magnetic force of the external electromagnetic field; such nondipole corrections are of the order of v/c, that is much larger than the dynamic relativistic effects due to the mass correction. This issue has been widely discussed in the literature (see, for example, Refs. [25,55–58]). We should note that the full form (45) of the interaction with the electromagnetic field beyond the dipole approximation violates invariance with respect to the nonrelativistic scaling (47) even if the system

is described by the TDSE. The vector potential in Eq. (45) depends on the variable

$$\eta = \omega t - \frac{\omega x}{c}. \qquad (50)$$

Upon the scaling transformation (47), the temporal part of this variable, ωt, remains invariant, while the spatial part $(\omega/c)x$ is multiplied by Z. Therefore one can expect more significant nondipole effects for the hydrogenlike ions with the larger nuclear charge Z.

In the other studies of nondipole effects in the relativistic atomic systems [8,10,11], numerical implementation was based on the separation of the spatial and temporal dependence in the vector potential by either the Fourier expansion or Taylor expansion in powers of x. With increasing intensity of the field, more and more expansion terms should be included to achieve convergence [12]. In our method, we apply the spatial and temporal dependence of the vector potential as it is and do not use any expansions. The Cartesian coordinate x, when expressed through the spherical coordinates,

$$x = r \sin \vartheta \cos \varphi, \qquad (51)$$

depends on the azimuthal angle φ. This angle is discretized on a uniform grid within the interval $[0, 2\pi]$. In the split-operator method, the external field propagator (22) is applied in the discretized φ representation. However, the angular-momentum representation is used to propagate the wave function with the unperturbed Hamiltonian propagator according to Eq. (20). To switch between the two representations, we apply the fast Fourier transform routines. Since we use a one-to-one mapping established by the discrete Fourier transform between the set of the discretized φ values and that of the angular-momentum projections, the number of φ grid points is equal to the number of angular-momentum projections retained in the wave function (13). The accuracy of the vector potential representation is thus controlled by the number of angular-momentum projections used. Of course, if a large number of φ grid points (or angular-momentum projections) is used, the calculations become very time consuming. However, if the nondipole corrections are not very large, usually a few m components in the wave function (13) are enough to obtain the results with reasonable accuracy.

In Fig. 4 we compare the ionization probabilities of H, Ne^{9+}, and Ar^{17+} calculated within and beyond the dipole approximation. Beyond the dipole approximation, we show the results for the angular-momentum projections $|m| \leqslant 2$ (BD2), $|m| \leqslant 3$ (BD3), and $|m| \leqslant 4$ (BD4) retained in the wave function (13). For the hydrogen atom, the dipole approximation (DA) is quite accurate for the field strengths up to 40 a.u. Even at $F = 60$ a.u., a deviation of BD2 and BD3 from the DA results is not large. On the other hand, a small discrepancy between the BD2 and BD3 results indicates that the convergence of the calculations beyond the dipole approximation can be achieved with relatively moderate number of φ grid points or angular-momentum projections. The situation changes significantly for Ne^{9+} and Ar^{17+}. While for Ne^{9+} the dipole approximation is still good at $Z^{-3}F = 10$ a.u., and BD2 and BD3 data show only a small deviation from the DA results at $Z^{-3}F = 15$ a.u., for Ar^{17+} a discrepancy between the DA results on the one hand and BD2 and BD3 results on the other

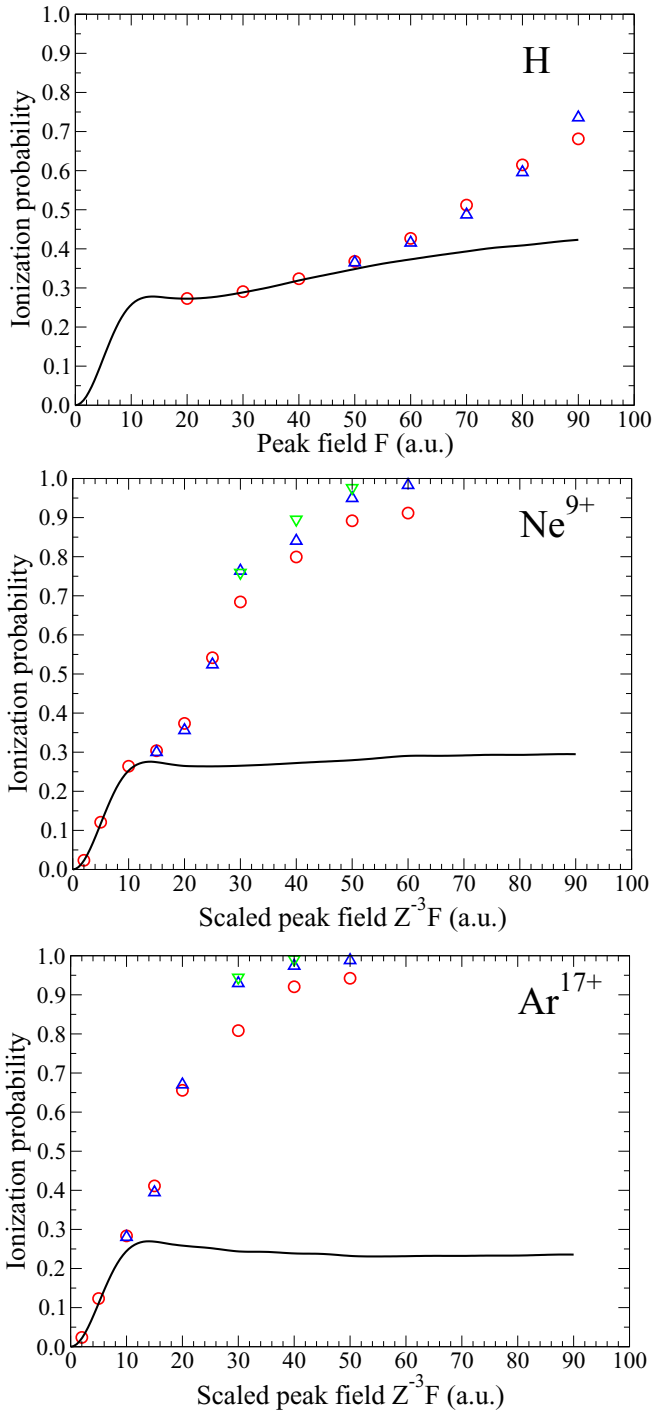FIG. 4. Ionization probabilities of H, Ne^{9+}, and Ar^{17+} calculated within and beyond the dipole approximation. Solid black line is the dipole approximation; red circles are BD2; blue triangles up are BD3; green triangles down are BD4 (see text for explanation). The carrier frequency is $\omega = 3.5Z^2$ a.u. and pulse duration $\tau = 2.5$ o.c.

hand is already quite large at $Z^{-3}F = 15$ a.u., indicating a breakdown of the dipole approximation. A difference between the BD2 and BD3 ionization probabilities remains small for the fields $Z^{-3}F \leqslant 25$ a.u. for Ne^{9+} and $Z^{-3}F \leqslant 20$ a.u. for Ar^{17+}. For stronger fields, this difference becomes larger. At the same time, a discrepancy between the BD3 and available

TABLE II. Lorentz deflection parameter Γ_R at the end of the dipole region of the field strength and scaled field strength $Z^{-3}F$ at $\Gamma_R = 1$.

Target	Scaled field $Z^{-3}F$ at $\Gamma_R = 1$ (a.u.)	Γ_R at end of dipole region
H	457	2.3×10^{-3} ($Z^{-3}F = 60$ a.u.)
Ne^{9+}	98	3.5×10^{-3} ($Z^{-3}F = 15$ a.u.)
Ar^{17+}	67	3.4×10^{-3} ($Z^{-3}F = 10$ a.u.)

BD4 results is still small at $Z^{-3}F \leqslant 30$ a.u., so we may expect convergence of the ionization probability calculations at the level BD3 for the scaled peak fields $Z^{-3}F$ less than or equal to 30 a.u. At stronger fields, convergence of the results beyond the dipole approximation at the level BD3 is not guaranteed. However, it is evident that the nondipole effects in these hydrogenlike ions in strong fields favor ionization. When the accuracy is improved by including more angular-momentum projections in the wave function, the ionization probability generally becomes larger. Since at $Z^{-3}F = 50$ a.u. for Ne^{9+} and at $Z^{-3}F = 40$ a.u. for Ar^{17+} the BD3 ionization probability is already close to unity, we may expect almost full ionization at stronger fields in the converged data as well.

As already mentioned, the nondipole effects in the ionization of hydrogenlike ions in strong electromagnetic fields are mainly caused by the influence of the magnetic force of the external field. A measure of such an influence was introduced in Ref. [55] in the form of the Lorentz deflection parameter:

$$\Gamma_R = \frac{\sqrt{I_p U_p^3}}{3\omega c^2}, \tag{52}$$

where I_p is the ionization potential of the target and $U_p = F^2/(4\omega^2)$ is the ponderomotive potential of the external field. If $\Gamma_R \geqslant 1$, then the rescattering electron misses the parent ion due to deflection by the magnetic force, thus manifesting a failure of the traditional strong-field ionization picture based on the dipole approximation. Therefore it is expected that the dipole approximation works well if $\Gamma_R \ll 1$. It is instructive to calculate the Lorentz deflection parameter for the targets used in our calculations and the field strengths where the numerical results suggest a transition between the dipole and nondipole ionization regimes. In Table II we present such results. First, we list the scaled field $Z^{-3}F$ values at $\Gamma_R = 1$. As one can see, these values are extremely large and lie far beyond the region where the dipole approximation is applicable according to our calculations. Therefore, $\Gamma_R = 1$ cannot be taken as a boundary between the dipole and nondipole ionization regimes. We determine the field strength corresponding to such a boundary approximately as the strongest field where the dipole approximation is still reasonably good, as seen in Fig. 4: $F = 60$ a.u. for the hydrogen atom, $Z^{-3}F = 15$ a.u. for Ne^{9+}, and $Z^{-3}F = 10$ a.u. for Ar^{17+}. As one can see in Table II, the resulting Γ_R values for all three targets are close to each other despite the substantial difference in the nuclear charge. We may conclude that, for the carrier frequency and pulse duration used in the present calculations, a region where the dipole approximation still works is limited to the Γ_R values of the order of 10^{-3} or less. At larger Γ_R, a significant

deviation of the accurate ionization probability from that calculated in the dipole approximation builds up.

IV. CONCLUSION

In this paper, we have performed a study of relativistic hydrogenlike ions subject to strong pulses of linearly polarized electromagnetic fields. To solve both the time-independent and time-dependent Dirac equations, we apply the generalized pseudospectral method in spherical coordinates. We suggest a transformation of the Dirac Hamiltonian in the spirit of the dual kinetic balance approach that removes the spurious eigenstates, which usually show up when solving the Dirac equation with the help of basis-set expansions. We calculate the ionization probabilities of the hydrogen atom as well as hydrogenlike neon and argon. For the hydrogen atom, we explore the dependence of the ionization on the pulse duration and find that larger ionization probability can be achieved with shorter pulses if the external field is strong enough. For Ne^{9+} and Ar^{17+}, the external field parameters in our calculations such as peak field strength, carrier frequency, and pulse duration are subject to scaling with respect to the nuclear charge. If the interaction with the external field is described within the dipole approximation and a nonrelativistic treatment is applied, then the same ionization probabilities are obtained for each hydrogenlike ion upon such a scaling. Deviation from this prediction indicates the importance of relativistic effects in the ionization process. All three hydrogenlike systems exhibit similar patterns in the dependence of the ionization probability on the peak field strength: a rapid growth of the ionization signal at weak fields is followed by a region of relative stabilization where the ionization probability changes only slightly on a wide range of the field strength. While in the weak-field region the relativistic effects in the ionization probability are quite small and can be attributed mostly to the relativistic increase of the ionization potential, in the strong-field region they are well pronounced for highly charged ions Ne^{9+} and Ar^{17+}. In this region, however, the dipole approximation itself becomes less accurate and eventually breaks down.

Our calculations beyond the dipole approximation show, as expected for the fixed carrier frequency and pulse duration, that the discrepancy between the dipole and nondipole results builds up as the peak field strength increases. The pattern in the dependence of the ionization probability on the peak field strength is changed qualitatively: instead of relative stabilization of the atomic system in strong fields seen within the dipole approximation, ionization probability now increases with the field strength. In the set of the hydrogenlike ions with the scaled field parameters, the nondipole corrections to the ionization probability grow with increasing nuclear charge. This is also expected since the full form of the interaction with the electromagnetic field beyond the dipole approximation violates the nonrelativistic scaling with respect to the nuclear charge, making the external field more nonuniform for the scaled system with the larger nuclear charge. While for the hydrogen atom we still see some stabilization plateau at relatively moderate field strengths, the highly charged ions Ne^{9+} and Ar^{17+} exhibit a rapid enhancement of the ionization when the field strength is increased, and the ionization probability approaches unity. Analysis of the dipole and nondipole numerical data for the ionization probability can help to set the limits of the applicability region of the dipole approximation. In this connection, we calculate the Lorentz deflection parameter proposed previously to estimate the nondipole effects due to the influence of the magnetic component of the external electromagnetic field. Based on our present results, we find that the dipole approximation works well if this parameter is of the order of 10^{-3} or less. Our analysis of the deflection parameter in this paper is limited to the specific carrier frequency and pulse duration. Generally, it would be desirable to perform a similar analysis for various laser pulse parameters. For example, one may expect that the deflection effect due to the magnetic field is more significant for longer pulses. However, such a comprehensive analysis is beyond the scope of the present paper. It requires large-scale calculations and could be a subject of further research.

[1] F. Krausz and M. Ivanov, Attosecond physics, Rev. Mod. Phys. **81**, 163 (2009).

[2] A. Di Piazza, C. Müller, K. Z. Hatsagortsyan, and C. H. Keitel, Extremely high-intensity laser interactions with fundamental quantum systems, Rev. Mod. Phys. **84**, 1177 (2012).

[3] T. Tschentscher and R. Feidenhans'l, Starting user operation at the European XFEL, Synchrotron Radiat. News **30**, 21 (2017).

[4] M. Dunne and B. Schoenlein, The Linac Coherent Light Source: Current status and future direction, Synchrotron Radiat. News **30**, 7 (2017).

[5] M. Vogel, W. Quint, G. Paulus, and T. Stöhlker, A penning trap for advanced studies with particles in extreme laser fields, Nucl. Instrum. Methods Phys. Res. Sect. B **285**, 65 (2012).

[6] S. Ringleb, M. Vogel, S. Kumar, W. Quint, G. G. Paulus, and T. Stöhlker, HILITE–ions in intense photon fields, Phys. Scr. **T166**, 014067 (2015).

[7] N. Stallkamp, S. Ringleb, B. Arndt, M. Kiffer, S. Kumar, T. Morgenroth, G. Paulus, W. Quint, T. Stöhlker, and M. Vogel, HILITE–A tool to investigate interactions of matter and light, X-Ray Spectrom. **49**, 188 (2020).

[8] S. Selstø, E. Lindroth, and J. Bengtsson, Solution of the Dirac equation for hydrogenlike systems exposed to intense electromagnetic pulses, Phys. Rev. A **79**, 043418 (2009).

[9] Y. V. Vanne and A. Saenz, Solution of the time-dependent Dirac equation for multiphoton ionization of highly charged hydrogenlike ions, Phys. Rev. A **85**, 033411 (2012).

[10] A. S. Simonsen, T. Kjellsson, M. Førre, E. Lindroth, and S. Selstø, Ionization dynamics beyond the dipole approximation induced by the pulse envelope, Phys. Rev. A **93**, 053411 (2016).

[11] T. Kjellsson, S. Selstø, and E. Lindroth, Relativistic ionization dynamics for a hydrogen atom exposed to superintense XUV laser pulses, Phys. Rev. A **95**, 043403 (2017).

[12] T. Kjellsson, M. Førre, A. S. Simonsen, S. Selstø, and E. Lindroth, Alternative gauge for the description of the light-matter interaction in a relativistic framework, Phys. Rev. A **96**, 023426 (2017).

[13] I. V. Ivanova, V. M. Shabaev, D. A. Telnov, and A. Saenz, Scaling relations of the time-dependent Dirac equation describing multiphoton ionization of hydrogenlike ions, Phys. Rev. A **98**, 063402 (2018).

[14] X.-M. Tong and S.-I Chu, Relativistic density-functional theory with the optimized effective potential and self-interaction correction: Application to atomic structure calculations ($Z = 2$–106), Phys. Rev. A **57**, 855 (1998).

[15] E. B. Rozenbaum, D. A. Glazov, V. M. Shabaev, K. E. Sosnova, and D. A. Telnov, Dual-kinetic-balance approach to the Dirac equation for axially symmetric systems: Application to static and time-dependent fields, Phys. Rev. A **89**, 012514 (2014).

[16] N. Moiseyev, Quantum theory of resonances: Calculating energies, widths and cross-sections by complex scaling, Phys. Rep. **302**, 212 (1998).

[17] S.-I Chu and D. A. Telnov, Beyond the Floquet theorem: Generalized Floquet formalisms and quasienergy methods for atomic and molecular multiphoton processes in intense laser fields, Phys. Rep. **390**, 1 (2004).

[18] M. S. Pindzola, J. A. Ludlow, and J. Colgan, Photoionization of highly charged atomic ions, Phys. Rev. A **81**, 063431 (2010).

[19] M. S. Pindzola, S. A. Abdel-Naby, F. Robicheaux, and J. Colgan, Single photoionization of highly charged atomic ions including the full electromagnetic-field potential, Phys. Rev. A **85**, 032701 (2012).

[20] I. A. Ivanov, Relativistic calculation of the electron-momentum shift in tunneling ionization, Phys. Rev. A **91**, 043410 (2015).

[21] H. Bauke, H. G. Hetzheim, G. R. Mocken, M. Ruf, and C. H. Keitel, Relativistic ionization characteristics of laser-driven hydrogenlike ions, Phys. Rev. A **83**, 063414 (2011).

[22] M. Klaiber, E. Yakaboylu, C. Müller, H. Bauke, G. G. Paulus, and K. Z. Hatsagortsyan, Spin dynamics in relativistic ionization with highly charged ions in super-strong laser fields, J. Phys. B: At. Mol. Opt. Phys. **47**, 065603 (2014).

[23] M. Klaiber and K. Z. Hatsagortsyan, Spin-asymmetric laser-driven relativistic tunneling from p states, Phys. Rev. A **90**, 063416 (2014).

[24] D. A. Tumakov, D. A. Telnov, G. Plunien, V. A. Zaytsev, and V. M. Shabaev, Relativistic mask method for electron momentum distributions after ionization of hydrogen-like ions in strong laser fields, Eur. Phys. J. D **74**, 188 (2020).

[25] H. R. Reiss, Dipole-approximation magnetic fields in strong laser beams, Phys. Rev. A **63**, 013409 (2000).

[26] M. Førre, J. P. Hansen, L. Kocbach, S. Selstø, and L. B. Madsen, Nondipole Ionization Dynamics of Atoms in Superintense High-Frequency Attosecond Pulses, Phys. Rev. Lett. **97**, 043601 (2006).

[27] M. Førre, S. Selstø, J. P. Hansen, T. K. Kjeldsen, and L. B. Madsen, Molecules in intense xuv pulses: Beyond the dipole approximation in linearly and circularly polarized fields, Phys. Rev. A **76**, 033415 (2007).

[28] Z. Zhou and S.-I Chu, Multiphoton above-threshold ionization in superintense free-electron x-ray laser fields: Beyond the dipole approximation, Phys. Rev. A **87**, 023407 (2013).

[29] T. E. Moe and M. Førre, Ionization of atomic hydrogen by an intense x-ray laser pulse: An *ab initio* study of the breakdown of the dipole approximation, Phys. Rev. A **97**, 013415 (2018).

[30] D. A. Telnov, D. A. Krapivin, J. Heslar, and S.-I Chu, Multiphoton ionization of one-electron relativistic diatomic quasimolecules in strong laser fields, J. Phys. Chem. A **122**, 8026 (2018).

[31] X.-M. Tong and S.-I Chu, Theoretical study of multiple high-order harmonic generation by intense ultrashort pulsed laser fields: A new generalized pseudospectral time-dependent method, Chem. Phys. **217**, 119 (1997).

[32] D. A. Telnov and S.-I Chu, Time-dependent generalized pseudospectral method for accurate treatment of multiphoton processes of diatomic molecules in intense laser fields, Comput. Phys. Commun. **182**, 18 (2011).

[33] D. A. Telnov, J. Heslar, and S.-I Chu, Effect of nuclear vibration on high-order-harmonic generation of aligned H_2^+ molecules, Phys. Rev. A **90**, 063412 (2014).

[34] D. A. Telnov and S.-I Chu, Minima in low-energy above-threshold-ionization spectra induced by electronic structure, Phys. Rev. A **100**, 043423 (2019).

[35] D. A. Telnov, J. Heslar, and S.-I Chu, Strong-field ionization of Li and Be: A time-dependent density functional theory with self-interaction correction, Chem. Phys. **391**, 88 (2011).

[36] D. A. Telnov, K. E. Sosnova, E. Rozenbaum, and S.-I Chu, Exterior complex scaling method in time-dependent density-functional theory: Multiphoton ionization and high-order-harmonic generation of Ar atoms, Phys. Rev. A **87**, 053406 (2013).

[37] K. Nasiri Avanaki, D. A. Telnov, and S.-I Chu, Harmonic generation of Li atoms in one- and two-photon Rabi-flopping regimes, Phys. Rev. A **94**, 053410 (2016).

[38] Y. Salamin, S. Hu, K. Hatsagortsyan, and C. Keitel, Relativistic high-power laser-matter interactions, Phys. Rep. **427**, 41 (2006).

[39] J. Crank and P. Nicolson, A practical method for numerical evaluation of solutions of partial differential equations of the heat-conduction type, Math. Proc. Cambridge Philos. Soc. **43**, 50 (1947).

[40] I. P. Grant, B-spline methods for radial Dirac equations, J. Phys. B: At. Mol. Opt. Phys. **42**, 055002 (2009).

[41] W. R. Johnson, S. A. Blundell, and J. Sapirstein, Finite basis sets for the Dirac equation constructed from B splines, Phys. Rev. A **37**, 307 (1988).

[42] E. Layton and S.-I Chu, Generalized Fourier-grid Hamiltonian approach to the Dirac equation: Variational solution without basis set, Chem. Phys. Lett. **186**, 100 (1991).

[43] V. M. Shabaev, I. I. Tupitsyn, V. A. Yerokhin, G. Plunien, and G. Soff, Dual Kinetic Balance Approach to Basis-Set Expansions for the Dirac Equation, Phys. Rev. Lett. **93**, 130405 (2004).

[44] C. Froese Fischer and O. Zatsarinny, AB-spline Galerkin method for the Dirac equation, Comput. Phys. Commun. **180**, 879 (2009).

[45] F. Fillion-Gourdeau, E. Lorin, and A. D. Bandrauk, Numerical solution of the time-independent Dirac equation for diatomic molecules: *B* splines without spurious states, Phys. Rev. A **85**, 022506 (2012).

[46] Q. Z. Lv, S. Norris, Q. Su, and R. Grobe, Numerical split-shift potential method for relativistic quantum systems with radial symmetry, J. Phys. B: At. Mol. Opt. Phys. **49**, 065003 (2016).

[47] F. A. Parpia and A. K. Mohanty, Relativistic basis-set calculations for atoms with Fermi nuclei, Phys. Rev. A **46**, 3735 (1992).

[48] D. V. Mironova, I. I. Tupitsyn, V. M. Shabaev, and G. Plunien, Relativistic calculations of the ground state energies and the critical distances for one-electron homonuclear quasi-molecules, Chem. Phys. **449**, 10 (2015).

[49] I. Angeli and K. P. Marinova, Table of experimental nuclear ground state charge radii: An update, At. Data Nucl. Data Tables **99**, 69 (2013).

[50] L. B. Madsen and P. Lambropoulos, Scaling of hydrogenic atoms and ions interacting with laser fields: Positronium in a laser field, Phys. Rev. A **59**, 4574 (1999).

[51] E. Tiesinga, P. J. Mohr, D. B. Newell, and B. N. Taylor, *The 2018 CODATA Recommended Values of the Fundamental Physical Constants* (web version 8.1), Database developed by J. Baker, M. Douma, and S. Kotochigova, Available at http://physics.nist.gov/constants, National Institute of Standards and Technology, Gaithersburg, MD 20899 (2020).

[52] M. Gavrila, Atomic stabilization in superintense laser fields, J. Phys. B: At. Mol. Opt. Phys. **35**, R147 (2002).

[53] M. Dondera, H. G. Muller, and M. Gavrila, Dynamic stabilization of ground-state hydrogen in superintense laser pulses of finite duration, Laser Phys. **12**, 415 (2002).

[54] M. Dondera, H. G. Muller, and M. Gavrila, Observability of the dynamic stabilization of ground-state hydrogen with super-intense femtosecond laser pulses, Phys. Rev. A **65**, 031405(R) (2002).

[55] S. Palaniyappan, I. Ghebregziabher, A. DiChiara, J. MacDonald, and B. C. Walker, Emergence from nonrelativistic strong-field rescattering to ultrastrong-field laser-atom physics: A semiclassical analysis, Phys. Rev. A **74**, 033403 (2006).

[56] H. R. Reiss, Limits on Tunneling Theories of Strong-Field Ionization, Phys. Rev. Lett. **101**, 043002 (2008).

[57] A. Ludwig, J. Maurer, B. W. Mayer, C. R. Phillips, L. Gallmann, and U. Keller, Breakdown of the Dipole Approximation in Strong-Field Ionization, Phys. Rev. Lett. **113**, 243001 (2014).

[58] M. Klaiber, K. Z. Hatsagortsyan, J. Wu, S. S. Luo, P. Grugan, and B. C. Walker, Limits of Strong Field Rescattering in the Relativistic Regime, Phys. Rev. Lett. **118**, 093001 (2017).